Available online at www.sciencedirect.com

ScienceDirect

Advances in Space Research 58 (2016) 2424–2434

ADVANCES IN SPACE RESEARCH (a COSPAR publication)

www.elsevier.com/locate/asr

GPS/UWB/MEMS-IMU tightly coupled navigation with improved robust Kalman filter

Zengke Li [a,b], Guobin Chang [a], Jingxiang Gao [a,*], Jian Wang [a], Alberto Hernandez [a]

[a] School of Environment and Spatial Informatics, China University of Mining and Technology, Xuzhou, China
[b] School of Information and Electrical Engineering, China University of Mining and Technology, Xuzhou, China

Received 23 October 2015; received in revised form 12 May 2016; accepted 21 July 2016
Available online 28 July 2016

Abstract

The integration of Global Positioning System (GPS) with Inertial Navigation System (INS) has been very intensively developed and widely applied in multiple areas. To further enhance the reliability and availability of GPS/INS integrated navigation in GPS challenging environment, range observation through ultra-wideband (UWB) is introduced in GPS/INS tightly coupled navigation. An improved robust Kalman filter is proposed and used to resist the influence of gross error from UWB observation in GPS/UWB/IMU tightly coupled navigation. The variance of the squared Mahalanobis distance in moving window is calculated, which brings as new judgement factor for gross errors in order to decrease the rate of false outlier identification. A simulation analysis shows that the improved robust Kalman filter is able to correctly identify gross errors and the rate of false judgment as zero. In order to validate the new robust filter, a real experiment is conducted. The results indicate that the improved robust Kalman filter used in GPS/UWB/INS tightly coupled navigation is able to remove the harmful effect of gross error in UWB observation. It clearly illustrates that the improved robust Kalman filter is very effective, and all the simulated small and large gross errors added to UWB distance observation are successfully identified.
© 2016 COSPAR. Published by Elsevier Ltd. All rights reserved.

Keywords: Ultra-wideband; Tightly coupled navigation; Robust Kalman filter; DGPS

1. Introduction

Integration between Global Positioning System (GPS) and Inertial Navigation Systems (INS) can be used for providing important and varied measurement information (position, velocity and attitude) (Chu et al., 2013). This has been investigated for several years in different applications, such as military (Barczyk and Lynch, 2012), agriculture (Li et al., 2012) and so on. In the integrated navigation and measurement system, GPS provides highly accurate position and velocity information over long periods, while INS provides accurate attitude measurement in the short term. When a GPS receiver is used to process position measurement, it needs to receive the satellite signal. In contrast, an INS is a self-contained device for velocity and attitude measurement. It is clear that integrating GPS and INS can deliver an enhanced performance over the individual system (Nassar and El-Sheimy, 2006).

When the satellite number is less than 4, tightly coupled mode can also be used by applying raw GPS data and data from INS mechanization algorithms in an integrated Kalman filter (Cox, 1978). So GPS/INS tightly coupled navigation is more flexible. Because the tightly coupled system was significantly more accurate, robust, jam-resistant, and less costly (Knight, 1996), a reconfigurable GPS/INS tightly coupled navigation filter was designed for spacecraft application (Upadhyay et al., 1993). Particle filtering which is a nonlinear/non-gaussian filter was tried in tightly coupled system in critical situations, which shown much supe-

* Corresponding author.
E-mail addresses: zengkeli@yeah.net (Z. Li), guobinchang@hotmail.com (G. Chang), jxgaocumt@yeah.net (J. Gao), wjiancumt@yeah.net (J. Wang), albert_h_m@hotmail.com (A. Hernandez).

http://dx.doi.org/10.1016/j.asr.2016.07.028
0273-1177/© 2016 COSPAR. Published by Elsevier Ltd. All rights reserved.

riority over extended Kalman filter (Radon-Nykodim, 1997). A fully digital airborne integrated mapping system (AIMS) for large-scale mapping and other high-precise positioning service was developed with GPS/INS tightly coupled technology (Grejner-Brzezinska et al., 1998). The INS prediction of positions and ionospheric effects were applied to approximate the new integer ambiguities if cycle slip occurred. An extended adaptive Kalman filtering algorithm was proposed based on the adaptive filter in tight coupled GPS/INS integration. The new algorithm cannot only resist the influence of the dynamic model errors, but also control the influence of the errors caused by the poor geometry of GPS satellites (Wu and Yang, 2010). A tightly coupled GPS/laser scanner/INS mechanization was developed and applied for trajectory reconstruction. The system architecture developed can exploit INS navigation states for improved solution robustness (Soloviev, 2010). A new fusion scheme of two-step adaptive robust filtering based on the observability of the parameters was developed for accuracy enhancement and error modification in tight integrated navigation. The INS errors could be accurately estimated and the accuracy of attitude angles was improved (Wu et al., 2012). Because of its advantage in size, price, and power consumption, micro-electro-mechanical system (MEMS) IMUs are now very popular in low-grade inertial systems (Barbour and Schmidt, 2001). The performance of a tightly coupled GPS/INS integrated system based on low cost MEMS IMUs in dense urban areas was evaluated, which indicated the potential of MEMS IMUs for use in land vehicle navigation applications (Godha and Cannon, 2007). System error and stability are the key problems for MEMS IMU. Different stochastic processes for modeling IMU sensor errors (Bhatti and Ochieng, 2007), such as random noise (Nassar and El-Sheimy, 2006), slowly growing error (Bhatti et al., 2012) and so no, are used to weaken INS positioning error. An enhanced tight cooperative positioning technique adding low-cost inertial navigation sensors and GPS Doppler shifts was proposed for improving the performance of absolute or relative positioning in a vehicular ad hoc network (VANET) (Alam et al., 2013). Recently, precise point positioning (PPP) has been developed using undifferenced carrier phase and pseudorange observations (Vaclavovic and Dousa, 2015) to obtain centimeter positions in static mode, after precise orbit and clock products became available (Kouba and Héroux, 2001). A new integrated navigation system was developed that integrated between-satellite single-difference (BSSD) PPP with a low-cost MEMS sensor-based inertial system. Decimeter-scale positioning accuracy could be achieved with undifferenced and BSSD integrated systems. However, in general, greater positioning accuracy was obtained using the BSSD integrated system (Rabbou and El-Rabbany, 2015).

The performance of GPS/INS integrated positioning and measurement will be seriously degraded in GPS challenging environments. To further enhance the reliability and availability of GPS/INS integration for measurement work, many researches on multi-sensor integration measurement and the corresponding algorithms have been performed. Ultra-wideband (UWB) has many advantages including signal robustness, resistance to frequency-selective fading, high communication capacity and fine-time resolution. UWB is of particular interest for positioning and tracking applications with distance measurements between radios because of the huge bandwidth available for time transfer (MacGougan et al., 2008). Several researches have been carried out to integrate UWB and GPS or INS, which would obtain more accurate position in GPS challenging environment. An augmented carrier-phase real-time kinematic (RTK) float filter was made that can be augmented with UWB range measurements. The UWB augmented solution shown a large improvement in terms of ratio and time of ambiguity fix (MacGougan et al., 2008). A system using low-cost UWB measurement system to augment GPS/MEMS (Micro-electromechanical Systems)-INS systems was proposed, of course in such an area where UWB positioning infrastructure was available. A multi-sensor fusion algorithm was developed, and it was obtained a dynamic position accuracy of 20 cm where UWB range measurements were available (Tanigawa et al., 2008). The GPS observations and ultra-wideband ranges tightly coupled system, which accounted for systematic UWB errors in real-time and additional error states, was introduced to an extended Kalman filter (EKF). Results of range measurements obtained by using commercially available UWB radios in optimal line-of-sight conditions were compared to surveyed ranges with conventional methods to assess UWB error characteristics (MacGougan and O'Keefe, 2009). An augmented low-cost GPS/INS navigation using impulse radio based on ultra-wideband transceivers in GPS challenged/denied areas for multi-platform relative navigation was proposed, and it was achieved an horizontal position accuracy of 0.5 m with robust performance of the system under GPS denied environments (Vydhyanathan et al., 2009). A tightly coupled integration between GPS and UWB observations for high accuracy position was tested to survey several external corner points of an eight-storey building. Sub-meter level position solutions were maintained using GPS/UWB integrated system (MacGougan et al., 2010b). An indoor navigation system was developed where the system architecture was based on the integration of UWB and inertial navigation (De Angelis et al., 2010). A commercially available UWB ranging system was employed in a tightly-coupled GPS and UWB RTK system. The integrated solution provided better accuracy, better ability to resolve integer ambiguities and enhanced fixed ambiguity solution availability compared with only GPS. Sub-decimetre accuracy was maintained in a degraded GPS environment (MacGougan et al., 2010a). A tightly coupled INS/UWB system for pedestrian indoor applications was presented. Combined with the integrity method, a robust integration has been implemented in

tightly coupled system (Ascher et al., 2011). The vehicle relative solution in Vehicle-to-Infrastructure (V2I) was implemented in an extended Kalman filter where differential GPS pseudorange and carrier phase measurements were used in conjunction with UWB ranges measured between the vehicle and two points at both sides of the road (Jiang et al., 2012). By exchanging GPS and UWB data between the vehicles, a form of collaborative positioning was obtained that provides improved performance over GPS alone (Petovello et al., 2012). A cooperative vehicle-to-vehicle (V2V) relative positioning approach was developed by using a federated filtering scheme in a Vehicular ad hoc Network (VANET) based on the techniques of differential GPS (DGPS) and UWB ranging. GPS pseudorange and Doppler and UWB range observations were used for V2V baseline estimation and achieved accuracy of 20–30 cm (Wang et al., 2013). Tightly-coupled fusion of DGPS and Impulse Radio UWB (IR-UWB) peer-to-peer ranging has been applied in relative navigation of aircraft in close formation-flight (Gross and Yu, 2014). To resolve the locations of a vehicle that was driving in Global Navigation Satellite System (GNSS) challenged/denied environments, a cooperative positioning solution using UWB and GNSS was developed. With UWB range observations, an accuracy better than decimetre could be achieved, even in a kinematic situation (Gao et al., 2014).

Building walls act as mirrors to UWB signals and receivers may measure AOA or TDOA of reflected signals, which would introduce large outlier in UWB range measurement (Pittet et al., 2008). Robust Kalman filter could be employed to resist the influence of gross error in UWB range measurement. Many forms of robust Kalman filter have been proposed in the literature. An adaptively robust filter was presented based on the robust maximum-likelihood estimation and applied in kinematic geodetic positioning and measurement. The method could not only balance the contribution between the updated parameters and measurement, but also resist the influence of measurement outliers (Yang et al., 2001). A new robust parameter estimator for the adjustment of correlated observations was developed based on a 'bifactor reduction' model of weight elements. The new equivalent weight matrix composed by the bifactor weight elements preserved the symmetry and kept the original correlation coefficients unchanged (Yang et al., 2002). An adaptively robust filter with multiple adaptive factors was proposed, based on the principles of adaptive Kalman filter and bifactor robust estimation for correlated observations. The adaptively robust filter with multiple adaptive factors and that with unified adaptive factor could be integrated in practical applications (Yang and Cui, 2008). Robust Kalman filter has been investigated over the past decades in different application areas, such as in-motion alignment of INS (Ali and Ushaq, 2009), SINS/SAR integrated navigation system (Gao et al., 2011), real-time estimation of satellite clock offset (Huang and Zhang, 2012), precise point positioning (PPP) (Guo and Zhang, 2014), small satellite attitude estimation (Soken et al., 2014), and so on. A robust KF using Chi square test to detect outliers in the measurement was proposed (Chang, 2014a). If the linear system with Gaussian-distributed white noise was correctly modeled, the observation vector should be Gaussian-distributed with mean and covariance being its prediction and the associate covariance. The square of the Mahalanobis distance from the observation to its prediction, which was defined as the test statistic as to detect outlier, should be Chi-square distributed with the dimension of the observation vector the same degree of freedom. Robust Kalman filter based on Mahalanobis distance is possible to cause false judgments.

In order to decrease false judgment rate, an improved robust Kalman filter is proposed and applied in GPS/UWB/INS tightly coupled navigation. The variance of the squared Mahalanobis distance is calculated in moving window and regarded as a new judgement factor for gross error in measurement system. The paper is divided into 5 sections. Following this introduction, the GPS/UWB/INS tightly coupled navigation model is overviewed in Section 2. Section 3 presents the improved robust Kalman filter, and the corresponding simulation analysis is showed. Field test results are then presented and analyzed in Section 4, followed by a summary of the main conclusions.

2. GPS/UWB/INS tightly coupled navigation

2.1. Dynamics model

The system error dynamic model of integrated navigation used in Kalman filter is developed based on the INS error equations. The insignificant terms are neglected in the process of linearization (Titterton, 2004). The psi-angle error equations of INS are as follows (Li et al., 2014):

$$\delta\dot{\boldsymbol{r}} = -\boldsymbol{\omega}_{en} \times \delta\boldsymbol{r} + \delta\boldsymbol{v} \tag{1}$$

$$\delta\dot{\boldsymbol{v}} = -(2\boldsymbol{\omega}_{ie} + \boldsymbol{\omega}_{en}) \times \delta\boldsymbol{v} - \delta\boldsymbol{\psi} \times \boldsymbol{f} + \boldsymbol{\delta} \tag{2}$$

$$\delta\dot{\boldsymbol{\psi}} = -(\boldsymbol{\omega}_{ie} + \boldsymbol{\omega}_{en}) \times \delta\boldsymbol{\psi} + \boldsymbol{\epsilon} \tag{3}$$

where $\delta\boldsymbol{r}$, $\delta\boldsymbol{v}$ and $\delta\boldsymbol{\psi}$ are the position, velocity and orientation error vectors, respectively. $\boldsymbol{\omega}_{en}$ is the rate of navigation frame with respect to earth, and $\boldsymbol{\omega}_{ie}$ is the rate of earth with respect to an inertial frame.

The accelerometer bias error vector $\boldsymbol{\delta}$ and the gyro drift error vector $\boldsymbol{\epsilon}$ are regarded as the random walk process vectors, which are modeled as follows:

$$\dot{\boldsymbol{\delta}} = \boldsymbol{\mu}_{\delta} \tag{4}$$

$$\dot{\boldsymbol{\epsilon}} = \boldsymbol{\mu}_{\epsilon} \tag{5}$$

where $\boldsymbol{\mu}_{\delta}$ and $\boldsymbol{\mu}_{\epsilon}$ are white Gaussian noise vectors.

By combining Eqs. (1)–(5), the dynamic system model becomes:

$$\begin{cases} \delta\dot{\boldsymbol{r}} = -\boldsymbol{\omega}_{en} \times \delta\boldsymbol{r} + \delta\boldsymbol{v} \\ \delta\dot{\boldsymbol{v}} = -(\boldsymbol{\omega}_{ie} + \boldsymbol{\omega}_{in}) \times \delta\boldsymbol{v} - \delta\boldsymbol{\psi} \times \boldsymbol{f} + \boldsymbol{\delta} \\ \delta\dot{\boldsymbol{\psi}} = -\boldsymbol{\omega}_{in} \times \delta\boldsymbol{\psi} + \boldsymbol{\epsilon} \\ \dot{\boldsymbol{\delta}} = \boldsymbol{\mu}_{\delta} \\ \dot{\boldsymbol{\epsilon}} = \boldsymbol{\mu}_{\epsilon} \end{cases} \tag{6}$$

which can be generalized in a matrix and vector form:

$$\dot{\boldsymbol{X}} = \boldsymbol{\Phi} X + \boldsymbol{\mu} \tag{7}$$

where $\boldsymbol{X}$ is the error state vector, $\boldsymbol{\Phi}$ is the state transition matrix, and $\boldsymbol{\mu}$ is the process noise vector.

2.2. Observation model

The observation model in GPS/INS/UWB tightly-coupled positioning scheme is composed of the pseudo-range and Doppler difference vector between the GPS observation and the INS computation value and the range difference between the UWB observation and the INS predication range:

$$\boldsymbol{Z} = \begin{bmatrix} P_j^{\mathrm{GPS}} - P_j^{\mathrm{INS}} & D_j^{\mathrm{GPS}} - D_j^{\mathrm{INS}} & r_i^{\mathrm{UWB}} - r_i^{\mathrm{INS}} & \cdots \end{bmatrix}^{\mathrm{T}} \tag{8}$$

where P_j^{GPS} and D_j^{GPS} are the pseudo-range and Doppler value observed by the jth GPS satellite, respectively; P_j^{INS} and D_j^{INS} are the pseudo-range and Doppler measurement of the jth satellite predicted by INS, respectively; r_i^{UWB} is the UWB ranging measurements of the ith UWB unit and r_i^{INS} is the distance calculated via the coordinates estimated using INS and the coordinates of the UWB reference stations. In order to improve the positioning accuracy of GPS, carrier phase smoothing technology is applied and precise ephemeris and clock products are used.

The generic measurement equation of the Kalman filter can be written as:

$$\boldsymbol{Z}_k = \boldsymbol{H}_k \boldsymbol{X}_k + \boldsymbol{w} \tag{9}$$

where $\boldsymbol{Z}_k$ is the m-dimensional observation vectors, $\boldsymbol{H}_k$ is the observation matrix (Farrell, 2008), and $\boldsymbol{w}$ is the measurement noise vector with covariance matrix $\boldsymbol{R}_k$, assumed to be white Gaussian noise.

3. Improved robust Kalman filter

3.1. Kalman filter

Based on the dynamics model and observation model, the Kalman filter is usually used to make information fusion in GPS/UWB/MEMS-IMU tightly coupled navigation. The optimal estimation of the state vector from the Kalman filter can be reached through a time update and a measurement update, which is independent of the measurements, is as follows at a time instant. The time update process is written as:

$$\bar{\boldsymbol{X}}_k = \boldsymbol{F}_{k,k-1} \hat{\boldsymbol{X}}_{k-1} \tag{10}$$

$$\bar{\boldsymbol{P}}_k = \boldsymbol{F}_{k,k-1} \boldsymbol{P}_{k-1} \boldsymbol{F}_{k,k-1}^{\mathrm{T}} + \boldsymbol{Q}_{k-1} \tag{11}$$

The observation update equation of Kalman filter is expressed as:

$$\bar{\boldsymbol{V}}_k = \boldsymbol{Z}_k - \boldsymbol{H}_k \bar{\boldsymbol{X}}_k \tag{12}$$

$$\boldsymbol{P}_{\bar{V}_k} = \boldsymbol{H}_k \bar{\boldsymbol{P}}_k \boldsymbol{H}_k^{\mathrm{T}} + \boldsymbol{R}_k \tag{13}$$

$$\boldsymbol{G}_k = \bar{\boldsymbol{P}}_k \boldsymbol{H}_k^{\mathrm{T}} \boldsymbol{P}_{\bar{V}_k}^{-1} \tag{14}$$

$$\hat{\boldsymbol{X}}_k = \bar{\boldsymbol{X}}_k + \boldsymbol{G}_k \bar{\boldsymbol{V}}_k \tag{15}$$

$$\boldsymbol{P}_k = (\boldsymbol{I} - \boldsymbol{G}_k \boldsymbol{H}_k) \bar{\boldsymbol{P}}_k \tag{16}$$

where $\bar{\boldsymbol{X}}_k$ is a priori state estimation, $\hat{\boldsymbol{X}}_k$ is a posteriori state estimation, $\boldsymbol{F}_{k,k-1}$ is the system matrix in discrete time form. $\boldsymbol{G}_k$ is the gain matrix of Kalman filter, $\bar{\boldsymbol{P}}_k$ is a priori covariance matrix of state vector, $\boldsymbol{P}_k$ is a posteriori covariance matrix of state vector, $\boldsymbol{R}_k$ is the covariance matrix of measurement noise vector, $\boldsymbol{Q}_{k-1}$ is the covariance matrix of process noise, the subscript k denotes the time, and the subscript $k, k-1$ represent the state and covariance estimates forward from k-1 time to k time.

3.2. Robust Kalman filter based on Mahalanobis distance

Under the Gaussian assumption, $\boldsymbol{Z}_k$ should be Gaussian with mean $\boldsymbol{H}_k \bar{\boldsymbol{X}}$ and covariance $\boldsymbol{P}_{\bar{V}_k}$. So the squared Mahalanobis distance of $\boldsymbol{Z}_k$ should be Chi square distributed (Chang, 2014b) and its freedom is the same as the m-dimensional of the observation vector $\boldsymbol{Z}_k$:

$$\gamma_k = M_k^2 = (\boldsymbol{Z}_k - \boldsymbol{H}_k \bar{\boldsymbol{X}})^{\mathrm{T}} (\boldsymbol{P}_{\bar{V}_k})^{-1} (\boldsymbol{Z}_k - \boldsymbol{H}_k \bar{\boldsymbol{X}}) \sim \chi_m^2 \tag{17}$$

where M_k is the Mahalanobis distance.

A Chi square test is constructed to judge whether the actual measurement is a realization of $\boldsymbol{Z}_k$ under the Gaussian assumption. A significant level α, a probability threshold below which the null hypothesis will be rejected, is selected. α is a small value. In this contribution 1% is adopted and the corresponding upper α-quantile is $\chi_{m,\alpha}^2$:

$$\Pr[\gamma_k > \chi_{m,\alpha}^2] < \alpha \tag{18}$$

where $\Pr[\cdot]$ represents the probability of a random event, i.e., that the probability of γ_k being larger than $\chi_{m,\alpha}^2$ should be very small, say α. So if the actual γ_k is larger than this α-quantile, the null hypotheses can be rejected and it can be concluded that there are some kinds of violations to the basic assumptions, and in this case, $\boldsymbol{Z}_k$ is deemed to be disturbed by gross error.

If the index γ_k is larger than $\chi_{m,\alpha}^2$, a robust factor β is introduced to inflate the covariance matrix of measurement noise vector:

$$\bar{\boldsymbol{R}}_k = \beta_k \boldsymbol{R}_k \tag{19}$$

The robust factor is calculated as (Chang, 2014a,b):

$$\beta_k = \frac{\gamma_k}{\chi_{m,\alpha}^2} \tag{20}$$

According to the above method, when γ_k is larger than $\chi^2_{m,\alpha}$, the observation $\boldsymbol{Z}_k$ is deemed to be disturbed by gross error. Actually, γ_k is possible to be larger than $\chi^2_{m,\alpha}$, even though there is no gross error in observation $\boldsymbol{Z}_k$. At the same time, the accuracy of innovation vector is also under the influence of process noise. Large process noise may result in that γ_k is larger than $\chi^2_{m,\alpha}$. So a looser threshold or more reliable judgment strategy is necessary for robust Kalman filter.

3.3. Improved robust Kalman filter

An improved robust Kalman filter is proposed using a more reliable judgment strategy based on the above robust Kalman filter. Because the squared Mahalanobis distance of $\boldsymbol{Z}_k$ should be Chi square distribute with m freedoms, the mean value and variance of γ_k are m and $2m$, respectively. A new judgment statistic for gross error is constructed as:

$$\lambda_k = \mathrm{var}(\gamma_{k-n} : \gamma_k) \tag{21}$$

where λ_k represents the variance of time series from γ_{k-n} to γ_k. Three times the variance of γ_k is used to determine a threshold T_D and then decide whether there are gross errors in the observations. If $\lambda_k > T_D$, the observation $\boldsymbol{Z}_k$ is deemed to be disturbed by gross error. The judgment statistic λ_k is the supplementary condition of Eq. (19). The detailed process of the improved robust Kalman filter is shown in Fig. 1.

The implementation of the improved robust Kalman filter is described step by step:

1. State $\bar{\boldsymbol{X}}_k$ prediction and corresponding covariance matrix $\bar{\boldsymbol{P}}_k$ calculation by Eqs. (10) and (11);
2. Innovation vector $\bar{\boldsymbol{V}}_k$ and corresponding covariance matrix $\boldsymbol{P}_{\bar{V}_k}$ calculation by Eqs. (12) and (13);
3. Calculating the index γ_k by Eq. (17);
4. Robust filter
   - 4.1. If $\gamma_k > \chi^2_{m,\alpha}$, calculate the judgment statistic λ_k;
     - 4.1.1. If $\lambda_k > T_D$, calculate the robust factor β_k by Eq. (20), expanding the covariance matrix of measurement noise vector by Eq. (19) and calculating the innovation vector covariance matrix $\boldsymbol{P}_{\bar{V}_k}$, go to step 3;
     - 4.1.2. If $\lambda_k \leqslant T_D$, standard Kalman filter updating, end of the filter;
   - 4.2. If $\gamma_k \leqslant \chi^2_{m,\alpha}$, standard Kalman filter updating, end of the filter.

3.4. Simulation analysis

The two-dimensional kinematic navigation simulation with constant velocity is employed. The dynamic model can be written as:

$$\dot{\mathbf{X}} = \begin{bmatrix} \dot{p}_N \\ \dot{p}_E \\ \dot{v}_N \\ \dot{v}_E \end{bmatrix} = \begin{bmatrix} 0 & 0 & 1 & 0 \\ 0 & 0 & 0 & 1 \\ 0 & 0 & 0 & 0 \\ 0 & 0 & 0 & 0 \end{bmatrix} \begin{bmatrix} p_N \\ p_E \\ v_N \\ v_E \end{bmatrix} + \begin{bmatrix} l0 \\ 0 \\ \alpha_N \\ \alpha_E \end{bmatrix} = \boldsymbol{\Phi} X + \boldsymbol{\mu} \tag{22}$$

where p_N, p_E, v_N and v_E are the position, velocity in the north and east directions, respectively, α_N and α_E are the north and east accelerations regarded as random noise in constant velocity model. The discrete time form of dynamical model is as follows:

$$\boldsymbol{X}_k = \boldsymbol{F}_{k,k-1}\boldsymbol{X}_{k-1} + \boldsymbol{\mu}_k \tag{23}$$

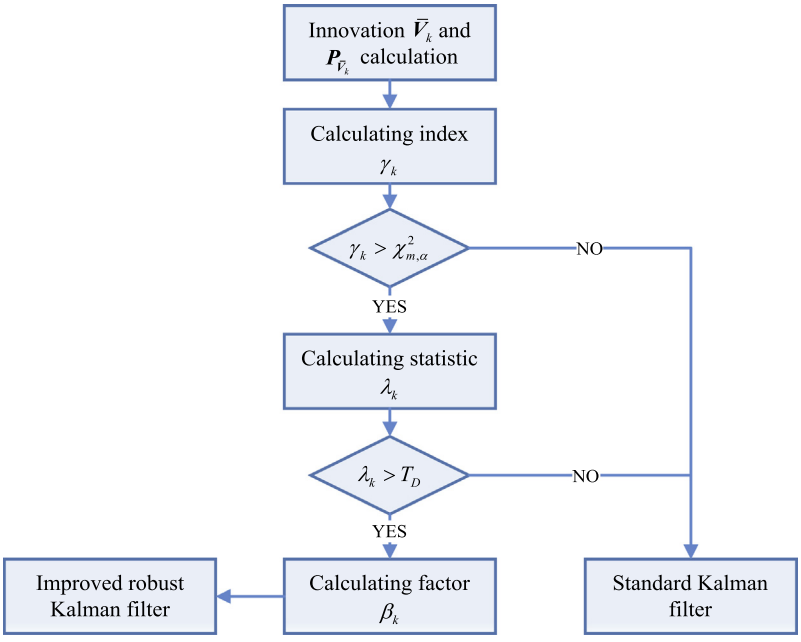

Fig. 1. The flow diagram of improved robust Kalman filter.

The observation information of simulation test is the distance between three fixed points and $\boldsymbol{X}$, so the observation model of Kalman filter is:

$$\boldsymbol{Z}_k = \begin{bmatrix} l_1 \\ l_2 \\ l_3 \end{bmatrix}_k = \mathbf{H}_k \begin{bmatrix} p_N \\ p_E \\ v_N \\ v_E \end{bmatrix} + \mathbf{w}_k \tag{24}$$

where l_1, l_2 and l_3 are the distance observations. The meaning of the other notations are the same as the Eq. (9).

The process noise $\boldsymbol{\mu}$ and observation noise $\boldsymbol{w}$ obey a Gaussian distribution. The standard deviation of process noise and observation noise are set as 0.15 m/s^2 and 1 m, respectively. In order to test the probabilities of false alarm by Eq. (18), no gross error case (case 1) and gross error case (case 2) are studied:

(1) There is no gross error in observation and standard Kalman filter (scheme 1), robust Kalman filter (scheme 2) and improved robust Kalman filter (scheme 3) are employed;
(2) Gross error with the value of -20 m is added into the distance observation l_1 every 200 s and gross error with the value of 15 m is added into all distance observations every 350 s. Similarly, three schemes are employed.

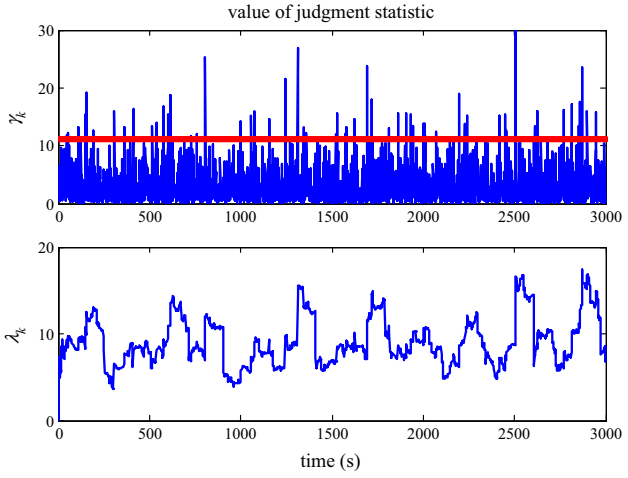

Fig. 2. Value of judgement statistic for gross error from different filter schemes.

The values of the judgment statistic γ_k and λ_k for case 1 are presented in Fig. 2. Although there is no gross error in observation, forty-three values of γ_k are greater than the threshold value 11.3 (red line). At the same time, all the values of λ_k are less than the threshold value 18. The analysis shows that the single judgment factor γ_k for gross error is possible to cause false-positive judgments. The error rate of false-positive judgment is about 2.30% in this simulation analysis. If the judgment statistic γ_k and λ_k are combined to identify gross error, the error rate of false-positive judgments is zero. Fig. 3 plots the position error series for different schemes in case 1. Table 1 illustrates root mean square (RMS) of position error of three schemes. Because the improved robust Kalman filter is able to identify gross error correctly, there is no false-positive judgment for scheme 3. The position error of scheme 1 and scheme 3 are the same in case 1. There is false-positive judgment with a 2.30 percent, so the position accuracy of scheme 2 is slightly poorer than the position accuracy of scheme 3. One obvious difference for three schemes is marked with a red circle.

Fig. 4 plots the position error series for different schemes in case 2. Table 2 illustrates the RMS of position error of three schemes. Gross errors are added into the distance observation, so the position error for standard Kalman filter is large. Both scheme 2 and scheme 3 achieve fine robust performance. The position error of scheme 2 is slightly larger than the position accuracy of scheme 3, which indicates that the improved robust Kalman filter possesses better stability.

Table 1
RMS comparison of position error for different filter schemes without gross error.

Scheme	North (m)	East (m)
Standard filter	0.600	0.732
Robust filter	0.602	0.737
Improved robust filter	0.600	0.732

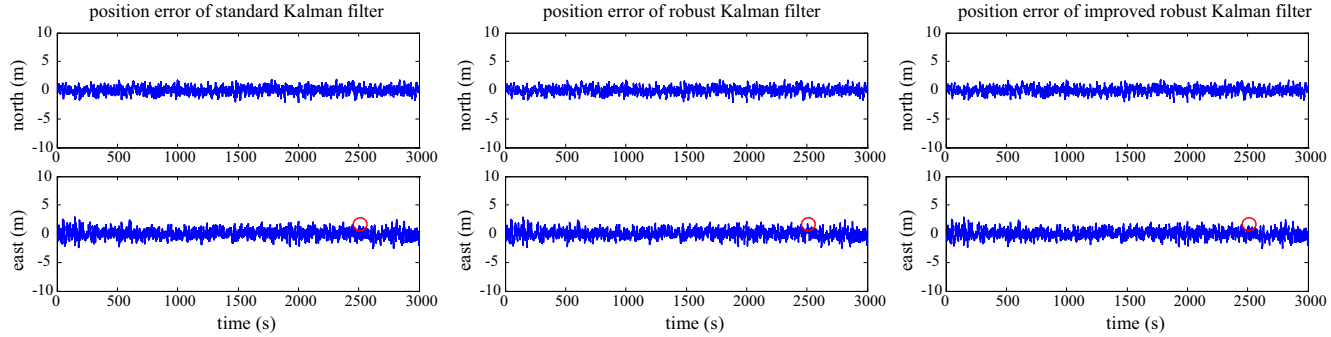

(a) standard Kalman filter (b) robust Kalman filter (c) improved robust Kalman filter

Fig. 3. Position error in north and east directions for different filter schemes without gross error.

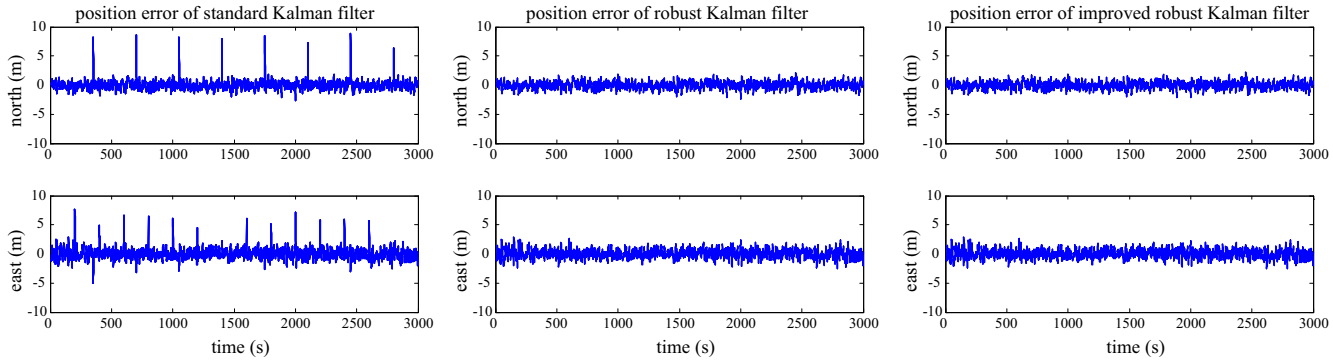

(a) standard Kalman filter (b) robust Kalman filter (c) improved robust Kalman filter

Fig. 4. Position error in north and east directions for different filter schemes with gross error.

Table 2
RMS comparison of position error for different filter schemes with gross error.

Scheme	North (m)	East (m)
Standard filter	0.818	0.933
Robust filter	0.607	0.745
Improved robust filter	0.605	0.741

Table 3
MEMS grade IMU technical data in field test.

Parameters	Gyroscope	Accelerometer
Initial bias error	±0.25°/s	±0.002 g
In-run bias stability	18°/h	±0.04 mg
Scale factor stability	±0.05%	±0.05 %
Random walk	0.03°/s/sqrt (Hz)	80 μg/sqrt (Hz)

4. Field test and analysis

Field tests were conducted to evaluate the performance of the proposed scheme on the roof of the Nottingham Geospatial Institute (NGI). The test consists of one MEMS grade IMU (Inertial Measurement Unit), one tactical grade IMU, 3 UWB units, and 2 GPS receivers. The sampling rate of the UWB unit was 1 Hz. In the beginning, a Leica AS10 GNSS dual-frequency antenna was installed on the top of a pillar above the NGI locomotive and a UWB unit was fastened under the antenna with a known lever-arm. Two UWB units were set on the pillars on the NGI roof and the coordinate of the pillars were known. The distance r_1^{UWB} and r_2^{UWB} between the locomotive and the pillars were measured by UWB. This UWB unit was also connected to a laptop to store the range observations. The MEMS IMU inside the locomotive was connected to the Leica antenna and recorded raw observations into a SD card for post-processing. Another GPS receiver was set on one of the pillars on the NGI roof to act as the reference station. As the UWB ranges were time tagged by the laptop system time, the laptop was synchronized to the GPS time to collect 1 Hz UWB ranges prior to the test. The sampling rate of GPS receivers and IMU were respectively configured as 10 Hz and 200 Hz.

The whole time of the test was about 20 min. The GPS observation was processed using the GPS software GrafNav™ 8.0 in DGPS mode and the solution was regarded as the position and velocity reference. The attitude reference was generated by Inertial Explorer processing software using the observations from two GPS receivers and one tactical grade IMU. The specifications of the MEMS-IMU are given in Table 3. The experience trajectory and the devices used during the tests are presented in Fig. 5.

In the data processing, the initial parameters of the Kalman filter for the integrated navigation were determined based on experience. The initial position and velocity errors were set based on the accuracy of the initial information from GPS. The initial position errors were 1 m, 1 m and 2 m and the initial velocity errors were 0.1 m/s, 0.1 m/s and 0.5 m/s in NED (North-East-Down) directions, respectively. In order to avoid initial alignment error that interfered the navigation results of different schemes, transfer alignment method was used to obtain high-accuracy attitude information. So, the initial platform alignment errors were 0.01°, 0.01° and 0.1°. According to the measurement accuracy of IMU, the initial standard deviations of gyro and accelerometer biases were 15°/h and 600 mg, respectively. The initial standard deviation of GPS and UWB observation were 2.5 m and 0.3 m/s based on their previous statistics information. All the parameters are identical for different schemes to obtain a better comparison performance.

The performance of GPS/UWB/INS tightly coupled navigation is tested. Fig. 6 shows the comparison of PDOP value under 10° cut-off elevation angles between GPS/INS (scheme 1) and GPS/UWB/INS (scheme 2) tightly coupled navigation. Shown in Fig. 7 is the field test trajectories comparison between scheme 1 and scheme 2. Fig. 8 shows the time series of position errors in the north, east and down directions for two schemes. The root mean square (RMS) of position error of two schemes is presented in Table 4. It can be shown the UWB is able to improve the position accuracy of GPS/INS tightly coupled navigation

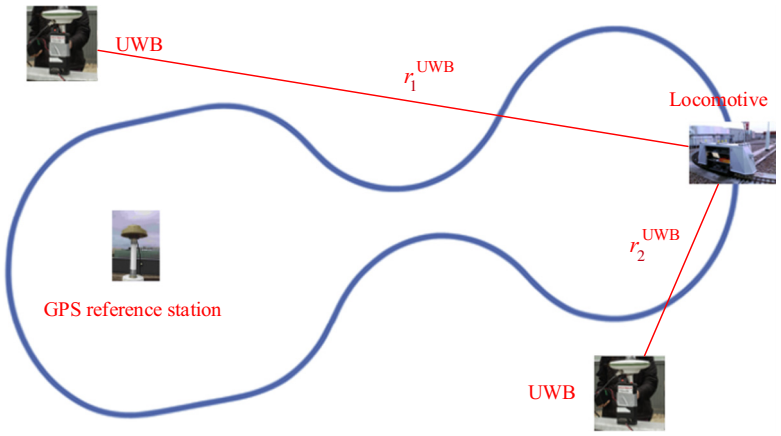

Fig. 5. Field test trajectory and instruments.

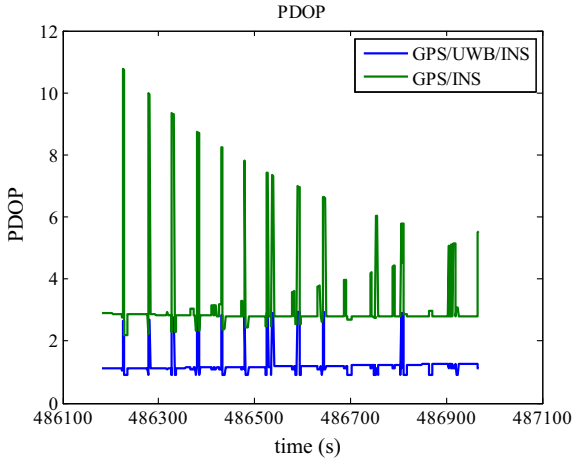

Fig. 6. PDOP value comparison between GPS/INS and GPS/UWB/INS tightly coupled navigation under 10° cut-off elevation angles.

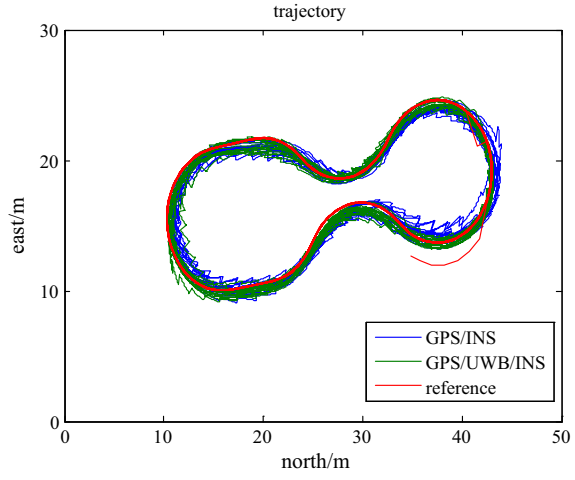

Fig. 7. Field test trajectories comparison between GPS/INS and GPS/UWB/INS tightly coupled navigation without gross error.

by 19%, 53% and 2% in the north, east and down directions. Because the UWB is installed above ground, it is not sufficiently effective to enhance the height positioning.

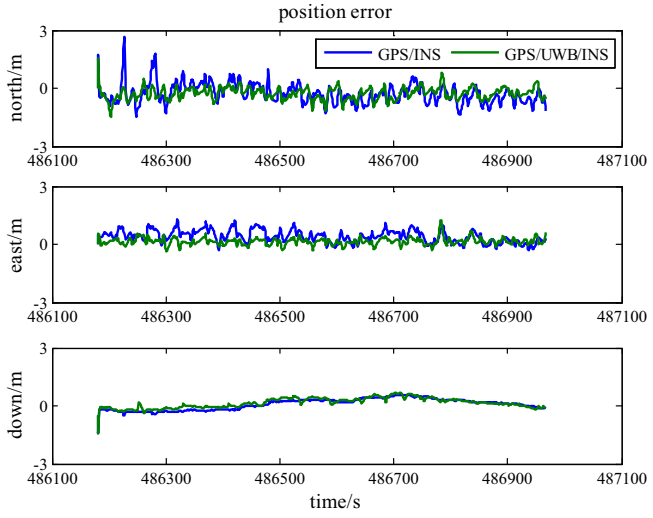

Fig. 8. Position error comparison between GPS/INS and GPS/UWB/INS tightly coupled navigation without gross error.

In order to test the improvement of UWB on GPS/INS integrated navigation during GPS blockage, one simulated blocked stretch of GPS satellite reception is introduced. Shown in Fig. 9 is the field test trajectories comparison between GPS/INS (scheme 1) and GPS/UWB/INS (scheme 2) tightly coupled navigation under the condition that all GPS signal are invalid between 486500 s and 486550 s (one lap time). This result is obvious and the position accuracy of scheme 2 is much better than that of scheme 1.

In order to test the performance of improved robust Kalman filter in GPS/UWB/MESM-IMU tightly coupled navigation, small gross error case (case 1) and large gross error case (case 2) are studied, and standard Kalman filter (scheme 1) and improved robust Kalman filter (scheme 2) are employed. Both small and large gross errors are randomly generated:

(1) Small gross errors with the value between 2 m and 5 m are added into two range observations of UWB r_1^{UWB} and r_2^{UWB} every 50 s.

Table 4
RMS comparison of position error between GPS/INS and GPS/UWB/INS tightly coupled navigation without gross error in field test.

Scheme	North (m)	East (m)	Down (m)
GPS/INS	0.517	0.515	0.301
GPS/UWB/INS	0.418	0.241	0.295

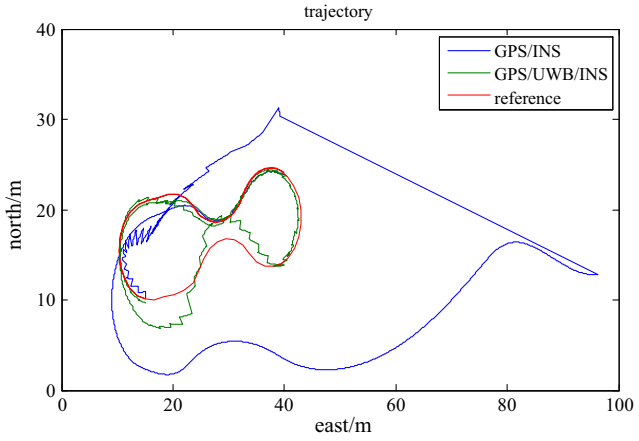

Fig. 9. Field test trajectories comparison between GPS/INS and GPS/UWB/INS tightly coupled navigation during all GPS signal blockage.

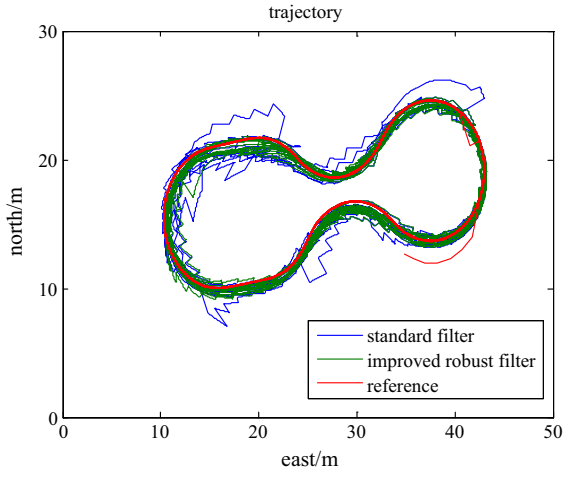

Fig. 10. Field test trajectories comparison between standard filter and improved robust filter with small gross error.

(2) Large gross errors with the value between 5 m and 10 m are added into two range observations of UWB r_1^{UWB} and r_2^{UWB} every 50 s.

In Fig. 10 it is shown a field test trajectories comparison for different schemes in case 1. Fig. 11 shows the time series of position errors in the north, east and down directions for scheme 1 and scheme 2. Table 5 illustrates root mean square (RMS) of position error of two schemes. The navigation resolution trajectory by standard Kalman filter seriously deviates from the reference. The improved Kalman filter is able to remove the ill effect from gross

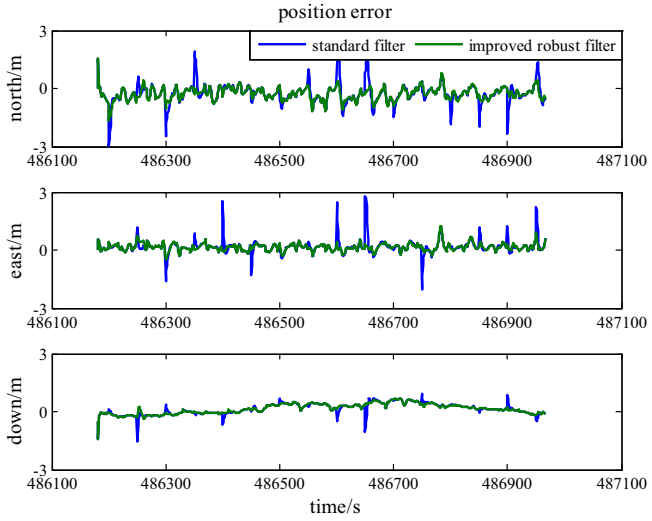

Fig. 11. Position error comparison between standard filter and improved robust filter with small gross error.

Table 5
RMS comparison of position error between standard filter and improved robust filter with small gross error.

Scheme	North (m)	East (m)	Down (m)
Standard filter	0.576	0.418	0.321
Improved robust filter	0.423	0.246	0.295

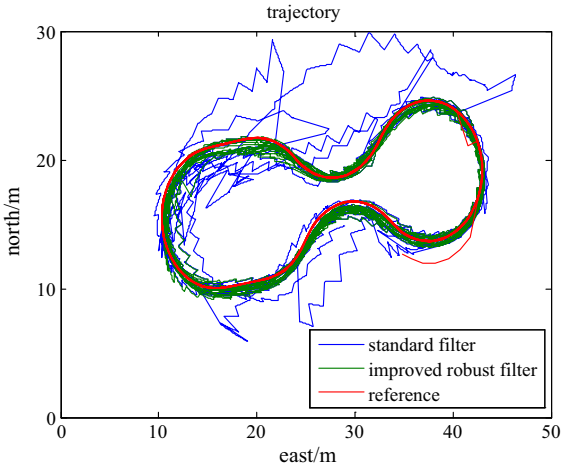

Fig. 12. Field test trajectories comparison between standard filter and improved robust filter with large gross error.

error. Compared to scheme 1, the proposed scheme 2 improves the position accuracy in the north, east and down directions by 27%, 41% and 8%, respectively. It clearly illustrates that the improved robust Kalman filter is very effective, and all the small gross errors are successfully identified.

Shown in Fig. 12 is a field test trajectories comparison for different schemes in case 2. Fig. 13 shows the time series of position errors in the north, east and down directions for scheme 1 and scheme 2. The root mean square (RMS) of

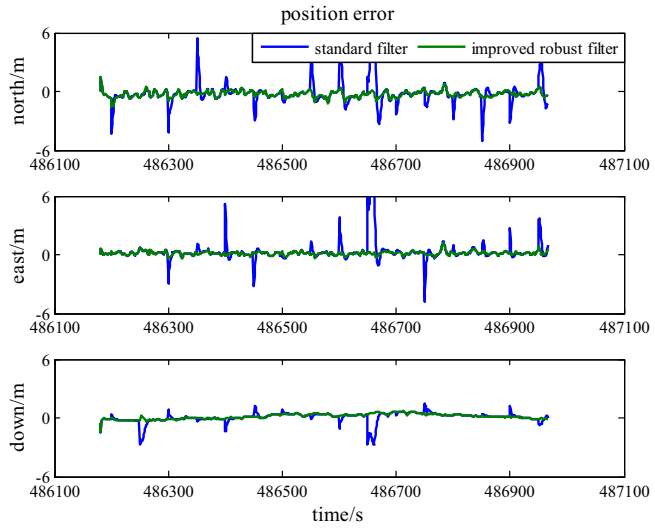

Fig. 13. Position error comparison between standard filter and improved robust filter with large gross error.

Table 6
RMS comparison of position error between standard filter and improved robust filter with large gross error.

Scheme	North (m)	East (m)	Down (m)
Standard filter	1.301	1.089	0.517
Improved robust filter	0.422	0.244	0.295

position error of two schemes is presented in Table 6. As the result for small gross errors, the improved robust Kalman filter is very effective on identifying large gross errors. The RMS of position errors in the north, east and down direction are 1.301 m, 1.089 m and 0.517 m, respectively, when the standard Kalman filter is used. On the contrary, the RMS of position errors are 0.422 m, 0.244 m and 0.295 m respectively, when the improved robust Kalman filter is applied. Compared with the scheme 1 (1.774 m), the 3D position error from scheme 2 dropped down to 0.570 m.

5. Conclusion

Robust Kalman filter based on Mahalanobis distance is possible to cause false-positive judgments. According to that, this paper proposes an improved robust Kalman filter. The variance of the squared Mahalanobis distance is calculated in moving window and regarded as new judgement factor for gross error detection. With the judging index based on Mahalanobis distance, a detailed implementation of the improved robust Kalman filter is presented.

Through the simulation analysis and comparison for the error of standard Kalman filter, robust Kalman filter based on Mahalanobis distance and the improved robust Kalman filter, Robust Kalman filter with judgment index based on Mahalanobis distance is possible to cause false-positive judgments, which will lead to poorer results than standard Kalman filter in case that there is no gross error in observation. Two judgment statistics are combined to identify gross errors in the improved robust Kalman filter and the error rate of false-positive judgments is zero.

UWB is a nice supplement to GPS/INS integrated navigation, especially in GPS challenging environments, while there are many gross errors in the range observation from UWB. The improved robust Kalman filter is employed in GPS/UWB/MEMS-IMU tightly coupled navigation to remove the harmful effect from gross error of UWB observation. The improved robust Kalman filter is very effective on identifying the simulated small and large gross error added to UWB distance observation, which has a good robustness performance.

Acknowledgments

The work is partially sponsored by the Fundamental Research Funds for the Central Universities (grant number: 2014ZDPY29) and partially sponsored by A Project Funded by the Priority Academic Program Development of Jiangsu Higher Education Institutions (grant number: SZBF2011-6-B35). The authors would like to thank Dr. Xiaolin Meng and all the experience members in the University of Nottingham, as well as helping with the collection of the field test data.

References

Alam, N., Kealy, A., Dempster, A.G., 2013. An INS-aided tight integration approach for relative positioning enhancement in VANETs. IEEE Trans. Intell. Transp. Syst. 14, 1992–1996.

Ali, J., Ushaq, M., 2009. A consistent and robust Kalman filter design for in-motion alignment of inertial navigation system. Measurement 42, 577–582.

Ascher, C., Zwirello, L., Zwick, T., et al., 2011. Integrity monitoring for UWB/INS tightly coupled pedestrian indoor scenarios. In: 2011 International Conference on Indoor Positioning and Indoor Navigation (IPIN), Guimaraes, pp. 1–6.

Barbour, N., Schmidt, G., 2001. Inertial sensor technology trends. IEEE Sens. J. 1, 332–339.

Barczyk, M., Lynch, A.F., 2012. Integration of a triaxial magnetometer into a helicopter UAV GPS-aided INS. IEEE Trans. Aerosp. Electron. Syst. 48, 2947–2960.

Bhatti, U.I., Ochieng, W.Y., 2007. Failure modes and models for integrated GPS/INS systems. J. Navig. 60, 327–348.

Bhatti, U.I., Ochieng, W.Y., Feng, S., 2012. Performance of rate detector algorithms for an integrated GPS/INS system in the presence of slowly growing error. GPS Solution 16, 293–301.

Chang, G., 2014a. Robust Kalman filtering based on Mahalanobis distance as outlier judging criterion. J. Geod. 88, 391–401.

Chang, G., 2014b. Kalman filter with both adaptivity and robustness. J. Process Contr. 24, 81–87.

Chu, H.J., Tsai, G.J., Chiang, K.W., et al., 2013. GPS/MEMS INS data fusion and map matching in urban areas. Sensors 13, 11280–11288.

Cox, D.B., 1978. Integration of GPS with inertial navigation systems. Navigation 25, 236–245.

De Angelis, A., Nilsson, J., Skog, I., et al., 2010. Indoor positioning by ultrawide band radio aided inertial navigation. Metrol. Meas. Syst. 17, 447–460.

Farrell, J., 2008. Aided Navigation: GPS with High Rate Sensors. McGraw-Hill Companies, New York.

Gao, S., Zhong, Y., Li, W., 2011. Robust adaptive filtering method for SINS/SAR integrated navigation system. Aerosp. Sci. Technol. 15, 425–430.

Gao, Y., Meng, X., Hancock, C.M., et al., 2014. UWB/GNSS-based cooperative positioning method for V2X applications. In: Proceedings of the 27th International Technical Meeting of The Satellite Division of the Institute of Navigation, ION GNSS+ 2014. Tampa, Florida. pp. 3212–3221.

Godha, S., Cannon, M.E., 2007. GPS/MEMS INS integrated system for navigation in urban areas. GPS Solution 11, 193–203.

Grejner-Brzezinska, D., Da, R., Toth, C., 1998. GPS error modeling and OTF ambiguity resolution for high-accuracy GPS/INS integrated system. J. Geod. 72, 626–638.

Gross, J.N., Yu, G., 2014. Dewberry Brandon. Tightly-coupled GPS/UWB-ranging for relative navigation during formation flight. In: Proceedings of the 27th International Technical Meeting of The Satellite Division of the Institute of Navigation, ION GNSS+ 2014. Tampa, Florida, pp. 1698–708.

Guo, F., Zhang, X., 2014. Adaptive robust Kalman filtering for precise point positioning. Meas. Sci. Technol. 25, 1–8.

Huang, G., Zhang, Q., 2012. Real-time estimation of satellite clock offset using adaptively robust Kalman filter with classified adaptive factors. GPS Solution 16, 531–539.

Jiang, Y., Petovello, M., O'Keefe, K., et al., 2012. Augmentation of carrier-phase DGPS with UWB ranges for relative vehicle positioning. In: Proceedings of the 25th International Technical Meeting of The Satellite Division of the Institute of Navigation, ION GNSS 2012. Nashville, TN, pp. 1568–1579.

Knight, D.T., 1996. Rapid development of tightly-coupled GPS/INS systems. In: IEEE 1996 Position Location and Navigation Symposium. IEEE, Atlanta, Georgia, pp. 300–305.

Kouba, J., Héroux, P., 2001. Precise point positioning using IGS orbit and clock products. GPS Solution 5, 12–28.

Li, Y., Efatmaneshnik, M., Dempster, A.G., 2012. Attitude determination by integration of MEMS inertial sensors and GPS for autonomous agriculture applications. GPS Solution 16, 41–52.

Li, Z., Wang, J., Li, B., et al., 2014. GPS/INS/Odometer integrated system using fuzzy neural network for land vehicle navigation applications. J. Navig. 67, 967–983.

MacGougan, G., O'Keefe, K., 2009. Real time UWB error estimation in a tightly-coupled GPS/UWB positioning system. In: Proceedings of the 2009 International Technical Meeting of The Institute of Navigation. Anaheim, CA, pp. 360–374.

MacGougan, G., O'Keefe, K., Chiu, D., 2008. Multiple UWB range assisted GPS RTK in hostile environments. In: Proceedings of the 21st International Technical Meeting of the Satellite Division of The Institute of Navigation, ION GNSS 2008. Savannah, GA, pp. 3020–3035.

MacGougan, G., O'Keefe, K., Klukas, R., 2010a. Tightly-coupled GPS/UWB integration. J. Navig. 63, 1–22.

MacGougan, G., O'Keefe, K., Klukas, R., 2010b. Accuracy and reliability of tightly coupled GPS/ultra-wideband positioning for surveying in urban environments. GPS Solution 14, 351–364.

Nassar, S., El-Sheimy, N., 2006. A combined algorithm of improving INS error modeling and sensor measurements for accurate INS/GPS navigation. GPS Solution 10, 29–39.

Petovello, M.G., O'Keefe, K., Chan, B., et al., 2012. Demonstration of inter-vehicle UWB ranging to augment DGPS for improved relative positioning. J. Global Position Syst. 11, 11–21.

Pittet, S., Renaudin, V., Merminod, B., et al., 2008. UWB and MEMS based indoor navigation. J. Navig. 61, 369–384.

Rabbou, M.A., El-Rabbany, A., 2015. Tightly coupled integration of GPS precise point positioning and MEMS-based inertial systems. GPS Solution 19, 601–609.

Radon-Nykodim, R., 1997. Optimal nonlinear filtering in GPS/INS integration. IEEE Trans. Aerosp. Electron. Syst. 33, 835–850.

Soken, H.E., Hajiyev, C., Sakai, S.-I., 2014. Robust Kalman filtering for small satellite attitude estimation in the presence of measurement faults. Eur. J. Control 20, 64–72.

Soloviev, A., 2010. Tight coupling of GPS, INS, and laser for urban navigation. IEEE Trans. Aerosp. Electron. Syst. 46, 1731–1746.

Tanigawa, M., Hol, J.D., Dijkstra, F., et al., 2008. Augmentation of low-cost GPS/MEMS INS with UWB positioning system for seamless outdoor/indoor positioning. In: Proceedings of the 21st International Technical Meeting of the Satellite Division of The Institute of Navigation, ION GNSS 2008. Savannah, GA, pp. 1804–1811.

Titterton, D., 2004. Strapdown Inertial Navigation Technology, second ed. MIT Lincoln Laboratory, Lexington, Massachusetts.

Upadhyay, T., Cotterill, S., Deaton, A.W., 1993. Autonomous GPS/INS navigation experiment for space transfer vehicle. IEEE Trans. Aerosp. Electron. Syst. 29, 772–785.

Vaclavovic, P., Dousa, J., 2015. Backward smoothing for precise GNSS applications. Adv. Space Res. 56, 1627–1634.

Vydhyanathan, A., Luinge, H., Tanigawa, M., et al., 2009. Augmenting low-cost GPS/INS with ultra-wideband transceivers for multi-platform relative navigation. In: Proceedings of the 22nd International Technical Meeting of The Satellite Division of the Institute of Navigation, ION GNSS 2009. Savannah, GA, pp. 547–54.

Wang, D., O'Keefe, K., Petovello, M.G., 2013. Decentralized cooperative navigation for vehicle-to-vehicle (V2V) applications using GPS integrated with UWB range. In: Proceedings of the ION 2013 Pacific PNT Meeting. Honolulu, Hawaii, pp. 793–803.

Wu, F.M., Yang, Y.X., 2010. An extended adaptive Kalman filtering in tight coupled GPS/INS integration. Surv. Rev. 42, 146–154.

Wu, F.M., Yang, Y.X., Zhang, L.P., 2012. A new fusion scheme for accuracy enhancement and error modification in GPS/INS tight integrated navigation. Surv. Rev. 44, 208–214.

Yang, Y., Cui, X., 2008. Adaptively robust filter with multi adaptive factors. Surv. Rev. 40, 260–270.

Yang, Y., He, H., Xu, G., 2001. Adaptively robust filtering for kinematic geodetic positioning. J. Geod. 75, 109–116.

Yang, Y., Song, L., Xu, T., 2002. Robust estimator for correlated observations based on bifactor equivalent weights. J. Geod. 76, 353–358.